JOURNAL OF VIROLOGY, June 1992, p. 3522–3530
0022-538X/92/063522-09$02.00/0

Vol. 66, No. 6

Identification and Characterization of a Coronavirus Packaging Signal

JENNIFER A. FOSMIRE, KYONGMIN HWANG, AND SHINJI MAKINO*

Department of Microbiology, The University of Texas at Austin, Austin, Texas 78712-1095

Received 13 January 1992/Accepted 6 March 1992

Previously, a mouse hepatitis virus (MHV) genomic sequence necessary for defective interfering (DI) RNA packaging into MHV particles (packaging signal) was mapped to within a region of 1,480 nucleotides in the MHV polymerase gene by comparison of two DI RNAs. One of these, DIssF, is 3.6 kb in size and exhibits efficient packaging, whereas the other, DIssE, which is 2.3 kb, does not. For more precise mapping, a series of mutant DIssF RNAs with deletions within this 1,480-nucleotide region were constructed. After transfection of in vitro-synthesized mutant DI RNA in MHV-infected cells, the virus product was passaged several times. The efficiency of DI RNA packaging into MHV virions was then estimated by viral homologous interference activity and by analysis of intracellular virus-specific RNAs and virion RNA. The results indicated that an area of 190 nucleotides was necessary for packaging. A computer-generated secondary structural analysis of the A59 and JHM strains of MHV demonstrated that within this 190-nucleotide region a stable stem-loop of 69 nucleotides was common between the two viruses. A DIssE-derived DI RNA which had these 69 nucleotides inserted into the DIssE sequence demonstrated efficient DI RNA packaging. Site-directed mutagenic analysis showed that of these 69 nucleotides, the minimum sequence of the packaging signal was 61 nucleotides and that destruction of the secondary structure abolished packaging ability. These studies demonstrated that an MHV packaging signal was present within the 61 nucleotides, which are located on MHV genomic RNA 1,381 to 1,441 nucleotides upstream of the 3′ end of gene 1.

Mouse hepatitis virus (MHV), a coronavirus, is an enveloped virus containing a 31-kb, single-stranded, positive-sense genomic RNA (23, 24). The virion is composed of four structural proteins. Three of these are integral envelope proteins: S (spike), M (membrane), and HE (hemagglutinin-esterase); and the fourth is an internal virus component N (nucleocapsid). N, a phosphoprotein of 50 kDa (46), binds to virion RNA (47), forming the helical nucleocapsid of the virion. In infected cells, MHV synthesizes seven to eight coronavirus-specific mRNAs ranging in size from 1.8 kb to genomic length; these have a 3′ coterminal, nested-set structure (21, 25) and an identical 5′-end leader sequence of 72 to 77 nucleotides (19, 22, 44). Only the 31-kb mRNA 1 is efficiently packaged into MHV virions. The other mRNA species are not detected in MHV particles (23, 31).

Although packaging (the interaction of viral proteins and RNA to form infectious particles) represents a crucial process of the coronavirus replication cycle, the nature of MHV RNA packaging remains largely undescribed. Recently, however, a preliminary understanding of the coronavirus packaging mechanism has been gained through the analysis of MHV defective interfering (DI) RNAs (35). When MHV was serially passaged in tissue culture at a high multiplicity of infection, a variety of DI RNAs of different sizes was detected (27, 33). These DI RNAs have been classified into three types according to replication and packaging abilities. One is DIssA RNA of nearly genomic size, which is efficiently packaged into virus particles and replicates even in the absence of helper virus infection (31). The second type consists of smaller DI RNAs, requiring helper virus functions for replication, that are not packaged efficiently into MHV particles (27, 31). The structure and multiplication mechanisms of DIssE RNA, the 2.3-kb prototype of the second DI RNA group, have been studied in detail (30–32). The third type of DI RNA also requires helper virus infection for its replication; however, it can be packaged efficiently (35). DIssF RNA, the prototype of the third MHV DI RNA type, is 3.6 kb in size and consists of five noncontiguous genomic regions, including the leader sequence and the 3′ end of the genome (35).

Because the inefficiently packaged group of DI RNAs includes members that are both larger and smaller than DIssF (27), which was packaged efficiently, it became evident that the reason smaller DI RNAs fail to package efficiently, a feature shared by subgenomic mRNAs, is not simply that they are too small for efficient packaging. Rather, differences in packaging ability are probably due to the presence or absence of a packaging signal. Here, packaging signal is defined as the *cis*-acting genomic sequence necessary for specific recognition and efficient packaging of viral RNA. Sequence analysis of MHV genomic RNA and DIssE and DIssF RNAs indicates that the packaging signal is present within a region of 1,480 nucleotides of nonoverlapping sequence, present in DIssF and absent in DIssE, consisting of domains III and IV and part of the 3′ end of domain II of DIssF (35) (Fig. 1). We have previously established a system in which complete cDNAs of DIssE and DIssF were cloned downstream of the T7 promoter. In vitro-synthesized DI RNAs made from each of these clones replicate efficiently when transfected into MHV-infected cells (30, 35). Utilizing this system, it was demonstrated that a hybrid DI RNA, comprising the insertion of the aforementioned nonoverlapping regions into DIssE, packaged efficiently (35). Using a similar experimental strategy, van der Most et al. recently mapped the packaging signal to within a 650-nucleotide fragment located near the 3′ end of the second open reading frame of the gene 1 (ORF 1b) (48). Their observation confirms and extends our previous data, as this

* Corresponding author.

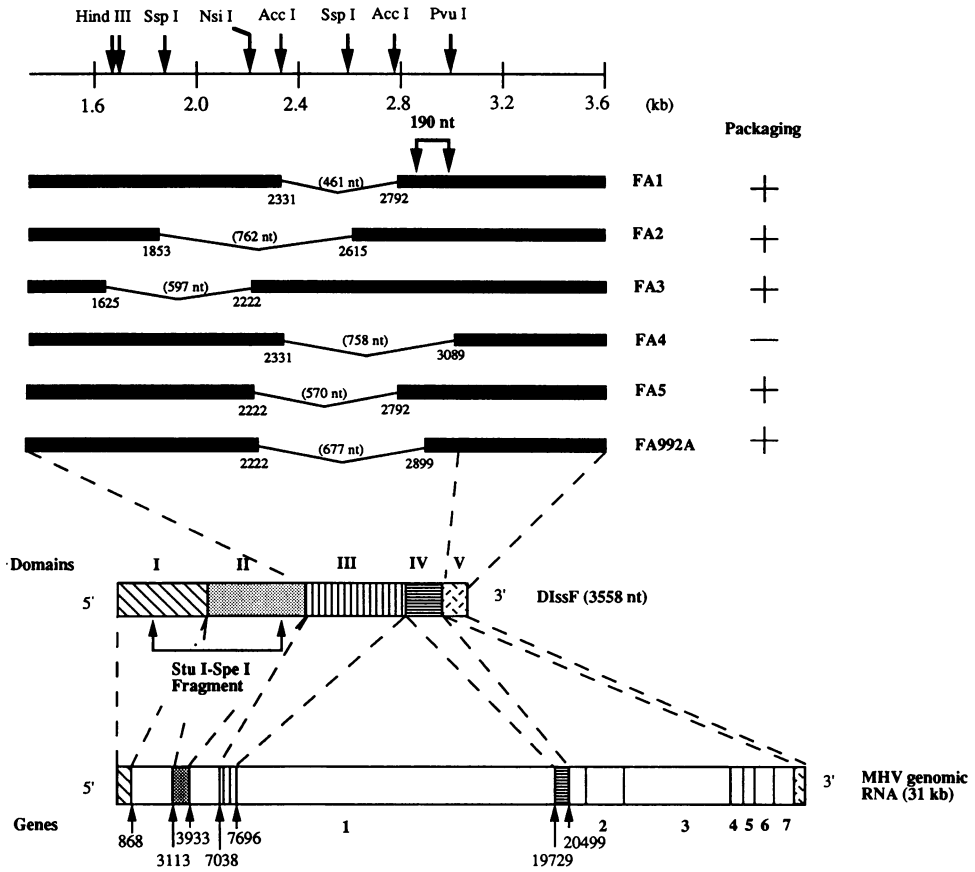

FIG. 1. Schematic diagrams of the structure of DIssF, DIssF-derived FA series deletion mutants, and MHV genomic RNA. The deleted sequences in FA1 through FA992A are shown as thin lines. The number above the thin line indicates the number of nucleotides deleted, and the exact location of the deleted regions is shown as nucleotides (nt) numbered from the 5′ end of DIssF. Restriction enzyme sites used in the construction of the deletion mutants are shown at the top of the diagram. The five domains of DIssF (domains I through V) are indicated above the diagram of DIssF; the exact location of I to IV on MHV genomic RNA is shown as nucleotides numbered from the 5′ end of MHV-JHM. A DIssF-derived *Stu*I-*Spe*I fragment was used for a probe for the experiments whose results are shown in Fig. 3A, 5A, and 6A. The numbers 1 through 7 represent the seven genes of MHV. The 190-nucleotide sequence noted above FA1 represents the region found to be important for packaging through the study of these mutants.

650-nucleotide region is included within domain IV of DIssF (35).

The experiments in this paper encompass the identification of a more detailed region of the MHV packaging signal by assessing the virus uptake of DIssF-derived mutant RNAs with internal deletions and DIssE-derived mutants with internal insertions. The MHV packaging signal was mapped to within 61 nucleotides located in MHV genomic RNA 1.4 kb from the 3′ end of gene 1, and site-directed mutagenic analysis indicated that the packaging signal secondary structure is important for function.

MATERIALS AND METHODS

Viruses and cells. The plaque-cloned A59 strain of MHV (MHV-A59) was used as a helper virus. Mouse L2 cells (21) and DBT cells (17) were used for propagation of virus.

Plasmid construction. (i) Construction of FA series mutants. DIssF-derived internal deletion mutants FA1 to FA5 were constructed by simply deleting internal regions of the complete DIssF cDNA clone DF 1-2 (35). Deletion sites of each deletion mutant are shown in Fig. 1. The deleted fragments for the mutants are as follows (name of mutant and deleted fragment): FA1, 461-nucleotide *Acc*I-*Acc*I fragment; FA2, 762-nucleotide *Ssp*I-*Ssp*I fragment; FA3, 597-nucleotide *Hin*dIII-*Nsi*I fragment; FA4, 758-nucleotide *Acc*I-*Pvu*I fragment; and FA5, 570-nucleotide *Nsi*I-*Acc*I fragment. FA992A was constructed by removing a 570-nucleotide *Nsi*I-*Acc*I fragment from DF 1-2 followed by exonuclease III-mung bean digestion proceeding in the 5′ to 3′ direction, from nucleotides 2792 to 2899, and subsequent self-ligation of the purified large DNA fragment. FA12 was constructed by inserting the 1.5-kb *Acc*I-*Sca*I fragment of MP-44 DIssF cDNA (35) into the 3.4-kb *Sca*I-*Sca*I fragment of the DIssE cDNA clone, DE5-w4 (30) (Fig. 2).

(ii) Construction of FB series mutants. In order to introduce mutations within the packaging signal, DIssF-derived DI cDNA MP 51-2 (28) (Fig. 2) was incubated with two oligonucleotides, 1167 (5′-AGCCATGCATCGAGCCATTA-3′), which binds to antigenomic-sense DIssF at nucleotides 2954 to 2973 from the 5′ end, and 1166 (5′-ACGTGATATCAGCT TCATTAC-3′), which binds to genomic-sense DIssF at nucleotides 3024 to 3043 from the 5′ end. The DNAs were incubated at 93°C for 30 s, 37°C for 45 s, and 72°C for 1 min and 40 s in a polymerase chain reaction (PCR) buffer (0.05 M KCl, 0.01 M Tris hydrochloride [pH 8.0], 0.0025 M $MgCl_2$,

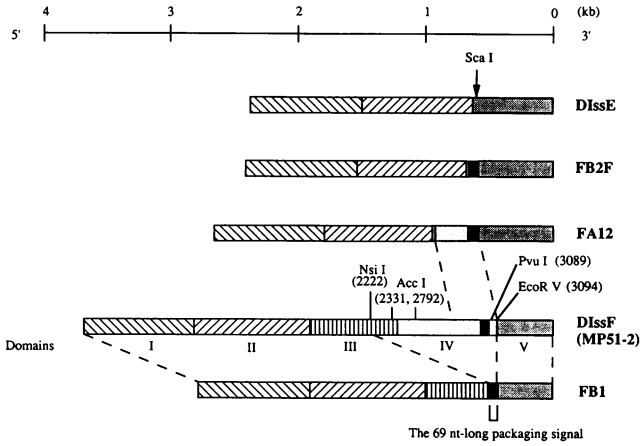

FIG. 2. Diagram of the structure of DIssE, DIssF-derived clone MP51-2 (28), FB2F, FA12, and FB1. The 69-nucleotide-long packaging signal is shown as black boxes. Restriction enzyme sites used for these constructions are shown above MP 51-2, with exact locations shown as nucleotides numbered from the 5′ end of MP 51-2.

0.01% gelatin, 0.17 mM [each] deoxynucleoside triphosphates, 5 U of *Taq* polymerase [Perkin Elmer Cetus]) for 25 cycles. The 75-nucleotide *Nsi*I-*Eco*RV fragment of the PCR product was inserted into the *Nsi*I-*Eco*RV site of MP 51-2, yielding FB1 (Fig. 2); thus, FB-1 is lacking nucleotides 2222 to 2957 and 3040 to 3101 compared with MP 51-2. Basically the same procedure was used for the construction of all FB mutants. The combination of oligonucleotides and the resulting mutants are listed (name of mutant, oligonucleotides binding to antigenomic-sense binding site on FB1, oligonucleotides binding to genomic-sense binding site on FB1, and template DNA for PCR) as follows: FB3, oligonucleotide 1230 (5′GACTATGCATCGAGCGTAATGGCGAGCCCA CAAGGT3′) (2218 to 2253), oligonucleotide 1166 (2288 to 2304), FB1; FB4, oligonucleotide 1227 (5′GACTATGCATC GAGCCATTACCGCTCCCCACA3′) (2218 to 2249), oligonucleotide 1166 (2288 to 2304), FB1; FB5, oligonucleotide 1231 (5′GACTATGCATCGAGCCATTACCGGAGGGGTG AAGGTA3′) (2218 to 2254), oligonucleotide 1166 (2288 to 2304), FB1; FB6, oligonucleotide 1392 (5′GACTATGCATC GAGCCATTACCGGAGCCCACAACTAAATCCGGGT GG3′) (2218 to 2264), oligonucleotide 1166 (2288 to 2304), FB1; FB7, oligonucleotide 1314 (5′AGTGGCAACGTCTTT TTA3′) (1781 to 1798), oligonucleotide 1389 (5′TTCTGAT ATCAGCTTGTAATGGCCTGAGATCACCCA3′) (2273 to 2308), FB1; FB8, oligonucleotide 1314 (1781 to 1798), oligonucleotide 1388 (5′TTCTGATATCAGCTTCATTACCGCT GAGATCAGGGTGGCGATTACCA3′) (2262 to 2308), FB1; FB12, oligonucleotide 1335 (5′GGGGACTATGCATCAT TACC3′) (2215 to 2239), oligonucleotide 130 (5′TTCCAAT TGGCCATGATCAA3′) (28) (2745 to 2754), FB1; FB13, oligonucleotide 1314 (1781 to 1798), oligonucleotide 1343 (5′TCTTTCTGATATCCATTACC3′) (2287 to 2311), FB1; and FB14, oligonucleotide 1335 (5′GGGGACTATGCATCA TTACC3′) (2215 to 2239), oligonucleotide 130 (2745 to 2754), FB 13. Vector EV-Q was created by inserting a *Hin*dIII-*Eco*RI fragment of DE5-w4 (30), which encompasses the entirety of DIssE including the T7 promoter and the poly(A) tail, into the *Sca*I site of pBR322. FB2F was constructed by inserting the 75-nucleotide *Nsi*I-*Eco*RV fragment of FB1 into the *Sca*I site of the DIssE sequence in EV-Q. For each mutant the entire region obtained by insertion of the PCR product was sequenced to confirm the presence of the specific mutations and the absence of extraneous mutations.

RNA transcription and transfection. Plasmids were linearized by *Xba*I digestion and transcribed in vitro with T7 RNA polymerase as described previously (30). For transfection of FA1, FA2, FA3, FA4, FA5, and FA12, DEAE-dextran-mediated transfection into L2 cells was performed as previously described (30, 31). For the transfection of other mutants, a lipofection procedure was used (11, 28). For both transfection procedures, 1 to 2 μg of RNA was transfected into 1.5×10^6 cells. Viruses were harvested at 12 to 15 h posttransfection and passaged without further dilution on DBT cells. Virus samples obtained from DI RNA-transfected cells are referred to as passage 0 virus samples.

Purification of viruses. Monolayers of confluent DBT cells (1.5×10^6 cells) were coinfected with 0.2 ml of MHV-A59 helper virus at a multiplicity of infection of 5 and 0.3 ml of passage 1 virus sample, which had been propagated from 1.5×10^6 DBT cells into 5 ml of culture medium. Viruses were labeled with $^{32}P_i$ according to published procedures and harvested at 12 h postinfection (p.i.) (33). After clarification by low-speed centrifugation, the supernatants were placed on discontinuous sucrose gradients consisting of 50 and 10% (wt/wt) sucrose in NTE buffer (0.1 M NaCl, 0.01 M Tris hydrochloride [pH 7.5], 0.001 M EDTA) and centrifuged at 26,000 rpm for 3 h at 4°C in a Beckman SW28 rotor. The virus band at the interface between 10 and 50% was collected, diluted with NTE buffer, and layered on a 20 to 60% continuous sucrose gradient for centrifugation at 26,000 rpm in a Beckman SW28 rotor for 17 to 21 h at 4°C. Fractions were collected from the bottom of the centrifuge tubes and examined for radioactivity by Cerenkov counting. For each virus sample, fractions representing the peak of radioactivity were pooled, diluted with NTE buffer, and pelleted by centrifugation at 38,000 rpm for 1 h at 4°C in a Beckman SW40 rotor.

Preparation of virion RNA and intracellular RNA. Virion RNA was extracted from purified viruses with phenol-chloroform (33). The intracellular virus-specific RNA was extracted as described previously (34).

Northern (RNA) blotting. For each sample, 1.5 μg of intracellular RNA was denatured and electrophoresed through a 1% agarose gel containing formaldehyde and transferred to a nylon membrane as previously described (28). After baking, the membrane was prehybridized at 42°C for 2 h in a buffer of 50% formamide, 0.1% Ficoll, 0.1% polyvinylpyrrolidone, 0.1% bovine serum albumin, 0.1% sodium dodecyl sulfate (SDS), 0.05 M sodium phosphate (pH 6.5)–5× SSC (1× SSC is 0.15 M NaCl plus 0.015 M sodium citrate), containing 100 μg of denatured nonhomologous DNA per ml. A DI-specific probe consisting of a ^{32}P-labeled *Stu*I-*Spe*I 1-kb fragment from the 5′ end of DIssF was prepared by a random priming labeling procedure (40). Labeled probe was denatured at 100°C for 10 min and added to the prehybridization solution, and hybridization proceeded with incubation at 42°C for 16 h. The membrane was washed three times in 2× SSC and 0.1% SDS at room temperature for 10 min and then twice at 50°C for 15 min, air dried, and exposed to Kodak XAR-5 film.

Agarose gel electrophoresis of virion RNA. ^{32}P-labeled virion RNA was electrophoresed in 1% agarose-formaldehyde gels (28). After electrophoresis, gels were washed three times with 0.1 M ammonium acetate for 20 min and then with water for 20 min once, dried by vacuum, and exposed to Kodak XAR-5 film.

RESULTS

Identification of the packaging signal. To more precisely define the location of the MHV packaging signal within the 1,480-nucleotide region unique to DIssF, a number of DIssF-derived mutants were constructed by restriction enzyme and exonuclease III-mung bean digestion within the DIssF-unique region (Fig. 1). Plasmids were linearized with *Xba*I, transcribed by T7 RNA polymerase in the presence of a cap analog [m7G(5′)ppp(5′)G] (30), and the resultant RNAs were transfected into L2 cells infected with MHV-A59 helper virus 1 h prior to transfection (30, 31). In vitro-synthesized DF 1-2 RNA, which is a complete cDNA clone of DIssF RNA, was used as a positive control (35), and mock transfection served as the negative control. After incubation of virus-infected cells at 37°C for 12 to 15 h, the culture fluid was harvested and cell debris were removed by low-speed centrifugation. This sample was named passage 0 virus sample and was used for inoculation of fresh DBT cells to obtain passage 1 virus sample. Passage 1 virus sample was used as the inoculum for the analysis of DI RNA replication and packaging ability. To examine the replication abilities of these mutant DI RNAs, intracellular RNA species were examined by Northern blot analysis for which the 1-kb *Stu*I-*Spe*I fragment of DF 1-2, which corresponds to part of MHV genomic gene 1, was used as a probe (Fig. 1). Thus, in this analysis, only genomic RNA and DI RNA were detectable. As shown in Fig. 3A, efficient replication of all DI RNAs was demonstrated. The amount of DI RNA was much more abundant than that of MHV genomic RNA, requiring a much longer exposure to detect genomic RNA (data not shown). To examine whether these DI RNAs were efficiently packaged into MHV particles, ^{32}P-labeled viruses harvested at 12 h p.i. were purified by sucrose gradient centrifugation. In all cases only a single peak of radioactivity, with a buoyant density of 1.19 g/cm^3, was observed after continuous sucrose gradient centrifugation (data not shown). The ^{32}P-labeled virion RNA was extracted from the pooled radioactive peak and analyzed by agarose gel electrophoresis. As shown in Fig. 3B, efficient packaging of DF 1-2, FA1, FA2, FA3, FA5, and FA992A into MHV particles was clearly demonstrated and the sizes of these DI RNAs were consistent with their predicted sizes. It was also evident that FA4 DI RNA was not packaged. Several additional bands, which are designated by asterisks in Fig. 3B, were detected in some viral RNA preparations. The RNA bands corresponding to these RNAs were also demonstrated after longer exposure of the Northern blot sample shown in Fig. 3A (data not shown), indicating that these are most probably new DI RNA species which were generated and accumulated during passage of virus samples. This analysis demonstrated that the deletion of nucleotides 1625 to 2899 had no adverse effect on DI RNA packaging, indicating that these bases are nonessential for MHV DI RNA packaging. Comparing the deletion of the nonpackaged mutant FA4 to the deletions of the other efficiently packaged mutants indicated that all or some of the 190 nucleotides between nucleotides 2899 and 3089 were necessary for packaging.

Previously it was shown that efficiently packaged MHV DI RNA accumulates in the virus population during serial undiluted passage of virus samples and interferes strongly with mRNA synthesis and infectivity of helper virus (35). Accumulation of MHV DI RNA was demonstrated by the fluctuation of helper virus infectivity during virus passages (35). To confirm that FA4 was not packaged efficiently into MHV particles, the passage 1 virus samples of all FA series

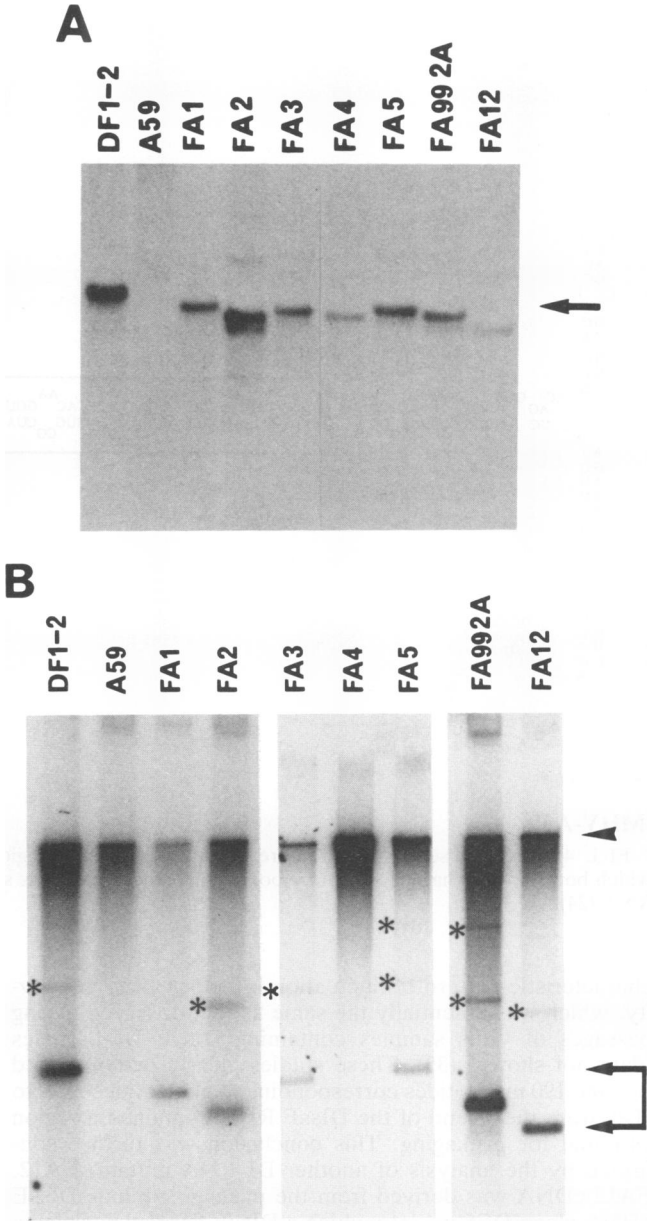

FIG. 3. Northern blot analysis of intracellular FA series DI RNA species and agarose gel electrophoresis of ^{32}P-labeled virion RNA. Viruses at passage level 1 were used for infection. (A) Intracellular RNAs were extracted at 7 h p.i., separated by 1% agarose-formaldehyde gel electrophoresis, and transferred to nylon membrane. DI RNA species were detected by using the *Stu*I-*Spe*I fragment (Fig. 1) as a probe. The arrow indicates DI RNA species. (B) ^{32}P-labeled virus released from DBT cells infected with passage 1 virus samples was purified, and virion RNA was extracted from purified virus particles. ^{32}P-labeled virion RNA species were analyzed by agarose-formaldehyde gel electrophoresis. The arrowhead indicates MHV-A59 genomic RNA. FA series DI RNA species migrated between the two arrows. RNA species marked with asterisks are most probably newly synthesized and accumulated DI RNA species generated during passage of virus samples.

DI particles were serially passaged without dilution on DBT cells, and the infectivity of virus samples at each passage level was determined. Only FA4 failed to show the infectivity fluctuation pattern, whereas the others demonstrated the

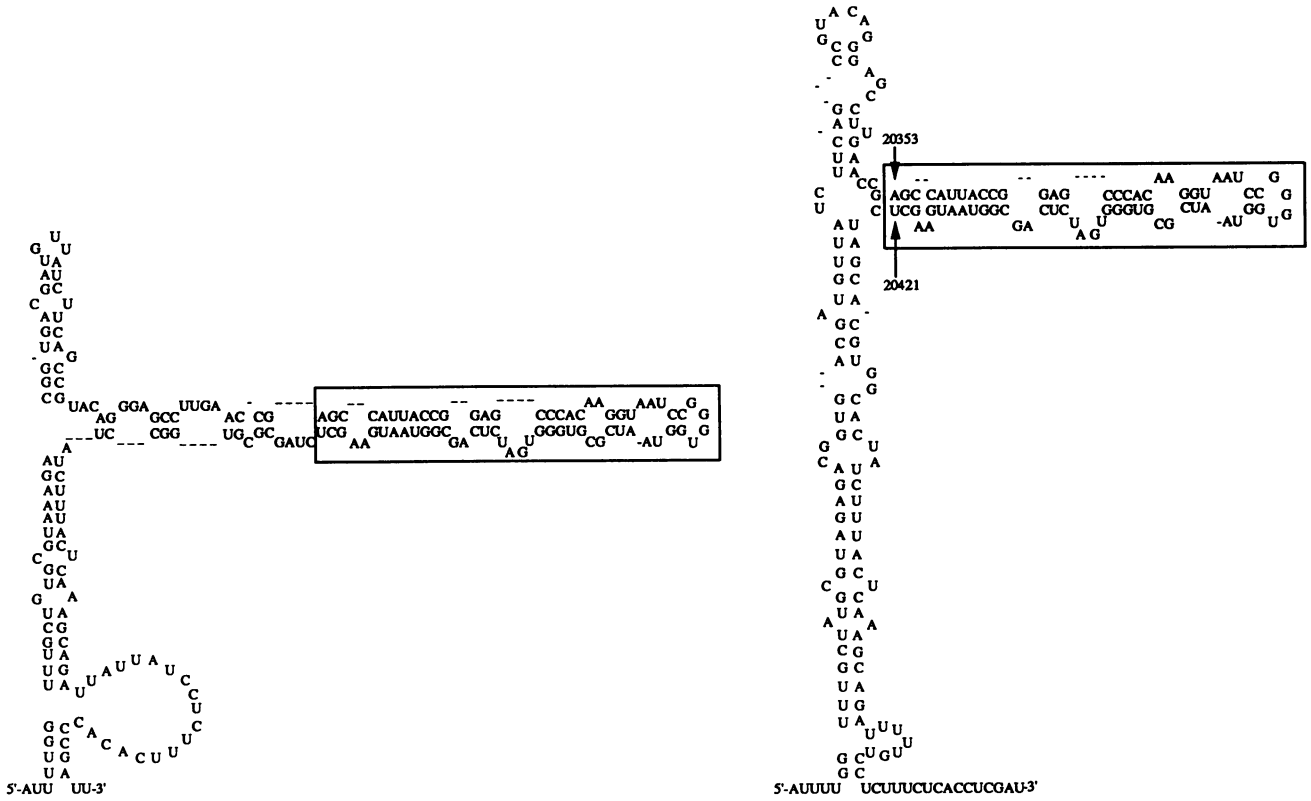

FIG. 4. Predicted secondary structure of the 190-nucleotide region of MHV-A59 and MHV-JHM. The 69-nucleotide stem-loop structure which both viruses share is shown by boxes; the exact location is shown as nucleotides numbered from the 5′ end of MHV-JHM genomic RNA (24).

characteristic pattern of fluctuation in helper virus infectivity, which was essentially the same as that observed during passages of virus samples containing DIssF DI particles (data not shown) (35). These studies clearly demonstrated that the 190 nucleotides corresponding to nucleotides 2899 to 3089 from the 5′ end of the DIssF RNA contained a region essential for packaging. This conclusion was further confirmed by the analysis of another DI RNA mutant, FA12. FA12 cDNA was derived from the packaging-minus DIssE cDNA clone DE5-w4 into which a DIssF-derived packaging signal was inserted at the *Sca*I site (Fig. 2). This packaging signal sequence originated from the 5′ end of a DIssF-derived fragment corresponding to nucleotides 2792 to 3089 (35). As shown in Fig. 3A and B, FA12 not only replicated efficiently but also packaged efficiently.

Secondary structural analysis of the 190-nucleotide-long packaging signal. It has been shown that the specific interaction between RNA and protein is frequently mediated by specific structures, i.e., the secondary or tertiary structure of RNA molecules (38). Therefore, the possibility of an important structural interaction existing between the 190-nucleotide packaging signal and nucleocapsid protein was investigated. Computer-based modeling (52) predicts that for both MHV-A59 (8) and MHV-JHM (24), this 190-nucleotide region produces a structure consisting of a main stem-loop with a smaller side stem-loop protruding from its side (Fig. 4). Although the structure of the main stem-loop was different between these two MHVs, the side stem showed striking similarities. The side stem-loop of MHV-A59 was longer than that of MHV-JHM, yet an identical structure was formed by the 69 nucleotides at the end of the side stem-loop of each virus (Fig. 4). This 69-nucleotide-long side stem-loop contained a series of highly complementary stems and mismatched bulges, with a small distal loop. Our present and previous studies have clearly demonstrated that the MHV-JHM-derived packaging signal is recognized by MHV-A59-derived packaging machinery; moreover, analysis of a number of MHV recombinant viruses has demonstrated that the exchange of this putative packaging signal between MHV-A59 and MHV-JHM does not affect particle formation (15, 16, 20, 26, 29). Therefore, it was assumed that this highly conserved portion was necessary and possibly sufficient for packaging function, and this 69-nucleotide side stem portion was studied in greater detail.

A 69-nucleotide sequence converts nonpackaged DI RNA to packaged DI RNA. To test the ability of the conserved side stem-loop structure to impart packaging properties to a previously nonpackaged DI RNA, the cDNA clone FB2F was constructed, in which only the 69-nucleotide side stem-loop was inserted at the *Sca*I site of a nonpackaged DIssE cDNA clone (Fig. 2). Efficient replication of FB2F DI RNA was demonstrated in passage 1 virus-infected cells (Fig. 5A). The packaging of FB2F DI RNA into MHV particles was examined by $^{32}P_i$ labeling of virus particles and subsequent sucrose gradient centrifugation. A single radioactive peak was again obtained after continuous sucrose gradient centrifugation (data not shown), and RNA from pooled peak fractions was separated by agarose gel electrophoresis to

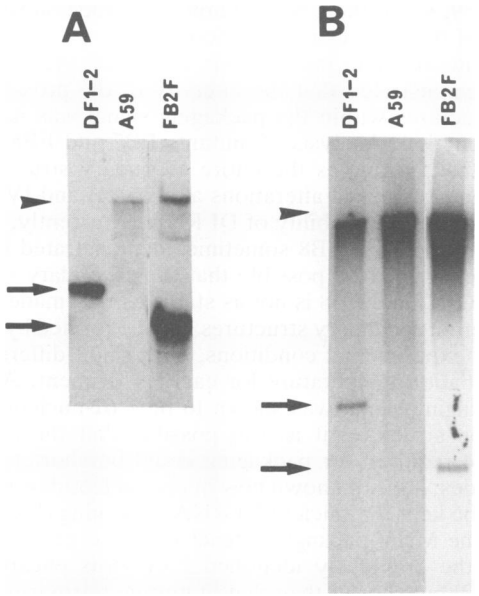

FIG. 5. Northern blot analysis of intracellular FB2F DI RNA species and agarose gel electrophoresis of ^{32}P-labeled virion RNA extracted from FB2F DI particles. Viruses at passage level 1 were used for infection. DF1-2 DI RNA (35) was shown as a positive control. (A) Intracellular RNAs were extracted at 7 h p.i., separated by 1% agarose-formaldehyde gel electrophoresis, and transferred to nylon membrane. DI RNA species were detected by using the *Stu*I-*Spe*I fragment (Fig. 1) as a probe. Arrows indicate DF1-2 DI RNA and FB2F DI RNA species, and an arrowhead indicates MHV genomic RNA. (B) ^{32}P-labeled virus released from DBT cells infected with passage-1 virus samples was purified, and virion RNA was extracted from purified virus particles. ^{32}P-labeled virion RNA species were analyzed by agarose-formaldehyde gel electrophoresis. MHV-A59 genomic RNA is shown by an arrowhead. DF1-2 DI RNA and FB2F DI RNA species are shown by arrows.

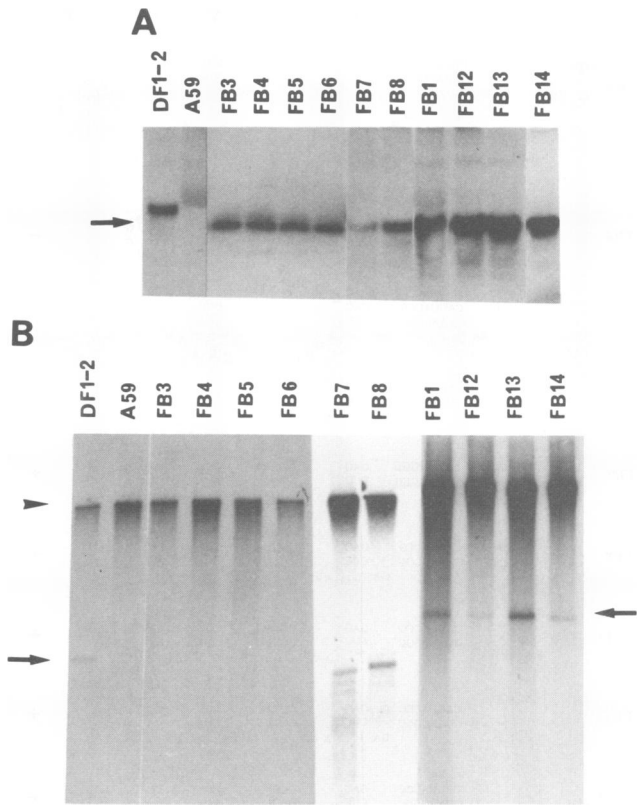

FIG. 6. Northern blot analysis of intracellular FB series DI RNA species and agarose gel electrophoresis of ^{32}P-labeled virion RNA. Viruses at passage level 1 were used for infection. (A) Intracellular RNAs were extracted at 7 h p.i., separated by 1% agarose-formaldehyde gel electrophoresis, and transferred to nylon membrane. DI RNA species were detected by using the *Stu*I-*Spe*I fragment (Fig. 1) as a probe. The arrow indicates DI RNA species. (B) ^{32}P-labeled virus released from DBT cells infected with passage 1 virus samples was purified, and virion RNA was extracted from purified virus particles. ^{32}P-labeled virion RNA species were analyzed by agarose-formaldehyde gel electrophoresis. The arrowhead indicates MHV-A59 genomic RNA. Arrows indicate FB series DI RNA species.

reveal that FB2F was efficiently packaged (Fig. 5B). This study clearly demonstrated that the packaging signal is located within this 69-nucleotide side stem-loop and that the 5′ and 3′ regions flanking this sequence are not necessary for DI RNA packaging.

Mutations in the side stem-loop change packaging properties. To further examine the nature of this packaging signal, a series of mutants were constructed to determine the relative importance of structure and sequence. For this analysis the FB1 clone was constructed as a wild-type clone. FB1 contains the 69-nucleotide side stem-loop inserted at nucleotides 2227 and 3100 of the DIssF-derived MP 51-2 clone; hence, 737 nucleotides from the 5′ end and 61 nucleotides from the 3′ end flanking regions of the 69-nucleotide-long packaging signal were deleted (Fig. 2). As shown in Fig. 6A and B, efficient replication and efficient packaging of FB1 were observed. Next, a series of FB1-derived mutant DI cDNAs with either altered secondary structure at each stem or an altered sequence that maintained the wild type-derived secondary structure were constructed by PCR-based site-directed mutagenesis. Destroying the structure of the proximal four highly complementary stems was accomplished by mutating the 5′ sequence of each stem to its respective 3′ complement; this resulted in large mismatched bulges replacing the stems (Fig. 7, FB3, FB4, FB5, and FB6). Mutants FB7 and FB8 restored the stem structure but changed the sequence of the second and fourth stems, respectively, by simultaneously exchanging the 5′ and 3′ sequences of the stems (Fig. 7). As shown in Fig. 6A, all these mutant DI RNAs replicated efficiently in MHV-A59-infected cells; however, in each case, loss of structural integrity resulted in a loss of packaging ability (Fig. 6B). In contrast to the results of the destruction mutants, mutants which have altered sequence but restored stem structure allowed efficient DI RNA packaging (Fig. 6B, FB7 and FB8). In some experiments we observed that the packaging efficiency of FB7 and FB8 was lower than that of FB1 (data not shown).

To determine whether 69 nucleotides is the minimum sequence which is required for efficient DI RNA packaging, three mutants, FB12, FB13, and FB14, were constructed. The structure of each mutant is shown in Fig. 7. Although all of these mutant DI RNAs packaged efficiently into MHV particles, the efficiency of FB12 and FB14 was often observed to be slightly lower than that of FB13 and FB1 (Fig. 6B). These studies demonstrated that the 3 nucleotides present at the 5′ end and the 5 nucleotides present at the 3′ end were not necessary for efficient MHV RNA packaging

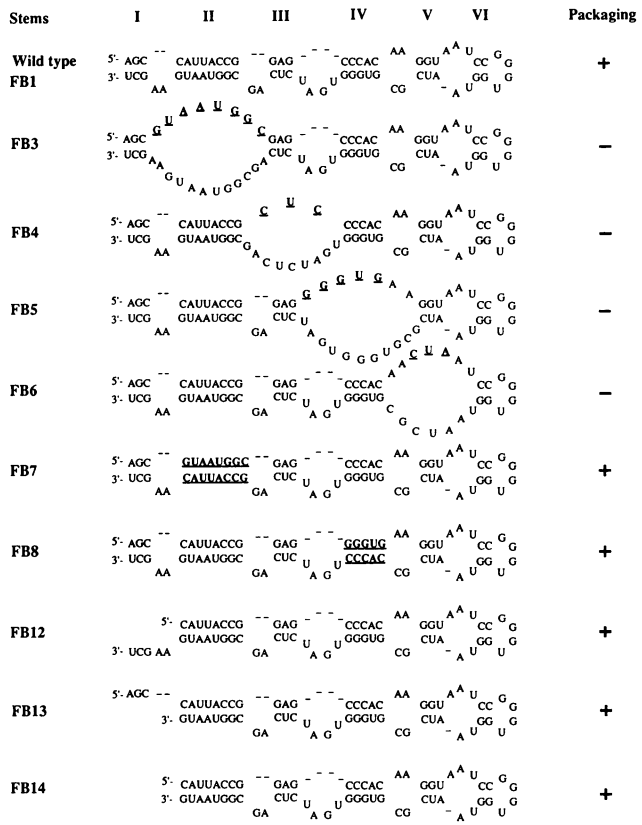

FIG. 7. Secondary structure of the 69-nucleotide-long packaging signal from the FB series DI RNAs. Altered nucleotides are underlined. Stem structures were named stems I to VI. +, efficiently packaged DI RNAs; −, poorly packaged DI RNAs.

(Fig. 7). Therefore, the packaging signal sequence was determined to be no longer than 61 nucleotides and was mapped at 20,356 to 20,416 nucleotides from the 5′ end of genomic RNA; thus, it is 1,381 to 1,441 nucleotides upstream from the 3′ end of gene 1 of MHV.

DISCUSSION

In the present study we have successfully identified a 61-nucleotide-long MHV packaging signal and mapped this to a position 1,381 to 1,441 nucleotides from the 3′ end of MHV gene 1. This conclusion was supported by the following observations: first, this 61-nucleotide-long sequence was included within two previously mapped putative packaging signal regions, 1,480 nucleotides and 650 nucleotides in length (35, 48); second, FB2F, which comprises the 69-nucleotide region including the 61-nucleotide-long sequence inserted into DIssE, demonstrated efficient packaging of its DI RNA; third, all MHV DI RNA deletion mutants lacking these 61 nucleotides also lacked the ability to package, whereas all other mutants containing these 61 nucleotides were packaged efficiently; fourth, deletion of 3 nucleotides at the 5′ end and 5 nucleotides at the 3′ end of the 69-nucleotide-long packaging signal of FB1 did not abolish packaging ability; fifth, deletion of the regions flanking the 61 nucleotides did not affect the packaging efficiency; and sixth, the sequence and structure made by the 61 nucleotides was completely conserved in two MHV strains, MHV-JHM and MHV-A59, while there are several nucleotide substitutions outside of the 61-nucleotide region.

The site-directed mutagenesis study of the packaging signal demonstrated that the integrity of the proximal four stem structures within the packaging signal was necessary for its function. Analysis of mutants FB7 and FB8 demonstrated that as long as the entire secondary structure was maintained, sequence alterations at stems II and IV did not affect the packaging ability of DI RNAs. Currently, it is not clear why FB7 and FB8 sometimes demonstrated less efficient packaging. It is possible that the secondary structure made by FB7 and FB8 is not as stable as that made by FB1 and different secondary structures may be formed by slightly different experimental conditions, e.g., slight differences in the incubation temperature for each experiment. Although the packaging signal was shown to be a 61-nucleotide-long stem-loop structure, it is also possible that the minimum sequence required for packaging could be shorter than 61 nucleotides; it is not known how many nucleotides of stem II need to be kept for efficient DI RNA packaging (Fig. 7). The size of the MHV packaging signal seems to be longer than that of the previously identified L-A virus encapsidation signal (12) but shorter than that of murine retroviruses (1, 2, 36, 37).

In the present study it was demonstrated that the packaging signal was necessary for MHV RNA packaging. However, it is not known whether this stretch of sequence is sufficient for MHV genomic RNA packaging. It is known that turnip crinkle virus (50) and Rous sarcoma virus (39, 43) have multiple encapsidation sites, which interact to produce packaging. Therefore, it would not be surprising that another region(s) of the MHV genome may also be necessary for RNA packaging. If such a sequence(s) exists, it should be present somewhere within domain I, II, or V of DIssF RNA. Because the N protein binds to MHV genomic RNA and forms a helical nucleocapsid, it is most likely that the packaging signal functions as an encapsidation site for N protein attachment on MHV genomic RNA. Previously, it was demonstrated that N protein binds to the leader sequence of all MHV mRNA species (3, 45). Therefore, it is possible that both the leader sequence and the 61-nucleotide-long packaging signal need to be recognized by packaging machinery for efficient packaging of MHV genomic RNA. Alternatively, the binding of N protein to the leader sequence may be important for MHV RNA synthesis but not for genomic RNA packaging, since it is known that N protein is also essential for MHV RNA replication in vitro (9) and synthesis of N protein is not inhibited even in the presence of DI particles (27). As shown in the present study, removal of the packaging signal did not affect DI RNA replication; thus, this signal was not considered to be a *cis*-acting element for MHV RNA replication. Further studies are necessary to determine whether the 61-nucleotide-long packaging signal identified in the present study is necessary and sufficient for MHV genomic RNA packaging.

Also unanswered is why the 61-nucleotide-long MHV packaging signal is located within ORF 1b, 1.4 kb from the 3′ end of gene 1. It is interesting that the putative GDD RNA polymerase motif begins 45 nucleotides upstream of the 61-nucleotide-long packaging signal (10). It has been shown that this GDD RNA polymerase motif and the flanking sequence of ORF 1b contain the active site of consensus RNA-dependent RNA polymerase sequences in several positive-stranded RNA viruses; however, it is not known whether this GDD RNA polymerase motif has MHV-specific RNA polymerase function (10). If this GDD RNA polymer-

ase motif is a functional RNA-dependent RNA polymerase and N protein specifically binds to the packaging signal, then the binding of N protein to the packaging signal may affect the translation of this RNA polymerase. It is conceivable that a large amount of N protein, which accumulates only late in infection, is necessary for the initiation of genomic RNA packaging and the binding of N to the packaging signal leads to the inhibition of GDD RNA polymerase translation. The inhibition of RNA polymerase synthesis may result in the reduction of MHV-specific RNA synthesis later during MHV infection. This speculation is consistent with the observation that MHV-specific RNA synthesis peaks at 6 h p.i. and then declines (41). Thus, it is possible that the packaging signal has another function affecting regulation of the MHV replication process. The possible role of an encapsidation site in RNA polymerase gene expression has been observed for other RNA viruses (5, 6, 49). It should be noted that the sequence necessary for the encapsidation of Sindbis virus genomic RNA, which is a positive-stranded RNA with GDD replicase, is mapped at the coding region of the nonstructural protein nsP1 (51). The RNA polymerase gene of Sindbis virus is mapped at nsP4 (4, 13, 14); therefore, it seems unlikely that the regulation of viral gene expression by the packaging signal is a general property of positive-stranded RNA viruses.

Sequence comparison of MHV genomic RNA and that of infectious bronchitis virus (IBV) reveals that the GDD motif is not present in the corresponding region of IBV sequence (7). Dot matrix comparison of the amino acid sequences of MHV-A59 and IBV demonstrated that the region surrounding the packaging signal has reduced amino acid similarity (8). Computer analysis of the IBV sequence in the region corresponding to the MHV packaging signal did not produce the stem-loop structure of MHV RNA (data not shown). These differences between MHV and IBV indicate that the packaging of IBV genomic RNA may require a different structure or sequence or that a packaging signal may be present in a different region of the genome. As discussed above, if the packaging signal has another function which regulates coronavirus RNA synthesis, then it is reasonable to speculate that the IBV-specific packaging signal may be located downstream of the IBV-specific RNA polymerase gene or another gene which has a function affecting RNA synthesis. It has been shown that gene order differs among the coronavirus genomic RNAs (18). It is, therefore, not surprising that the IBV packaging signal should be located at a different region on the genomic RNA compared with that of MHV. In addition, it should be noted that transmissible gastroenteritis virus genome may contain another packaging signal; subgenomic RNA species of transmissible gastroenteritis virus were detected in the purified transmissible gastroenteritis virus virion (42), although quantities of these subgenomic RNA species were not abundant. These observations may indicate that the location of the packaging signal and mechanisms regulating coronavirus RNA packaging may somehow differ among coronaviruses.

ACKNOWLEDGMENTS

We thank Jayne K. Makino for critical reading of the manuscript.

This work was supported by Public Health Service grant AI29984 from the National Institutes of Health. J.A.F. is supported by National Institutes of Health fellowship AI08520 from the National Institute of Allergy and Infectious Diseases.

REFERENCES

1. **Adam, M. A., and D. Miller.** 1988. Identification of a signal in a murine retrovirus that is sufficient for packaging of nonretroviral RNA into virions. J. Virol. **62:**3802–3806.
2. **Alford, R. L., S. Honda, C. B. Lawrence, and J. W. Belmont.** 1991. RNA secondary structure analysis of the packaging signal for Moloney murine leukemia virus. Virology **183:**611–619.
3. **Baric, R. S., G. W. Nelson, J. O. Fleming, R. J. Dean, J. G. Keck, N. Casteel, and S. A. Stohlman.** 1988. Interactions between coronavirus nucleocapsid protein and viral RNAs: implications for viral transcription. J. Virol. **62:**4280–4287.
4. **Barton, D. J., S. G. Sawicki, and D. L. Sawicki.** 1988. Demonstration in vitro of temperature-sensitive elongation of RNA in Sindbis virus mutant *ts*6. J. Virol. **62:**3597–3602.
5. **Bernardi, A., and P. F. Spahr.** 1972. Nucleotide sequence at the binding site for coat protein on RNA of bacteriophage R17. Proc. Natl. Acad. Sci. USA **69:**3033–3037.
6. **Berzin, V., G. P. Borisova, I. Cielens, V. A. Gribanov, I. Jansone, G. Rosenthal, and E. J. Gren.** 1978. The regulatory region of MS2 phage RNA replicase cistron: functional activity of individual MS2 RNA fragments. J. Mol. Biol. **119:**101–131.
7. **Boursnell, M. E. G., T. D. K. Brown, I. J. Foulds, P. F. Green, F. M. Tomley, and M. M. Binnis.** 1987. Completion of the sequence of the genome of the coronavirus avian infectious bronchitis virus. J. Gen. Virol. **68:**57–77.
8. **Bredenbeek, P. J., C. J. Pachuk, A. F. H. Noten, J. Charite, W. Luytjes, S. R. Weiss, and W. J. M. Spaan.** 1990. The primary structure and expression of the second open reading frame of the polymerase gene of the coronavirus MHV-A59; a highly conserved polymerase is expressed by an efficient ribosomal frameshifting mechanism. Nucleic Acids Res. **18:**1825–1832.
9. **Compton, S. R., D. B. Rogers, K. V. Holmes, D. Fertsch, J. Remenick, and J. J. McGowan.** 1987. In vitro replication of mouse hepatitis virus strain A59. J. Virol. **61:**1814–1820.
10. **Denison, M. R., P. W. Zoltick, J. L. Leibowitz, C. J. Pachuk, and S. R. Weiss.** 1991. Identification of polypeptides encoded in open reading frame 1b of the putative polymerase gene of the murine coronavirus mouse hepatitis virus A59. J. Virol. **65:** 3076–3082.
11. **Felgner, P. L., T. R. Gadek, M. Holm, R. Roman, H. W. Chan, M. Wenz, J. P. Northrop, G. M. Ringgold, and M. Danielson.** 1987. Lipofection: a high efficient, lipid-mediated DNA-transfection procedure. Proc. Natl. Acad. Sci. USA **84:**7413–7417.
12. **Fujimura, T., R. Esteban, L. M. Esteban, and R. B. Wickner.** 1990. Portable encapsidation signal of the L-A double-stranded RNA virus of S. cerevisiae. Cell **62:**819–828.
13. **Hahn, Y. S., A. Grakoui, C. M. Rice, E. G. Strauss, and J. H. Strauss.** 1989. Mapping of RNA$^-$ temperature-sensitive mutants of Sindbis virus: complementation group F mutants have lesions in nsP4. J. Virol. **63:**1194–1202.
14. **Kamer, G., and P. Argos.** 1984. Primary structural comparison of RNA-dependent polymerases from plant, animal and bacterial viruses. Nucleic Acids Res. **12:**7269–7282.
15. **Keck, J. G., G. K. Matsushima, S. Makino, J. O. Fleming, D. M. Vanner, S. A. Stohlman, and M. M. C. Lai.** 1988. In vivo RNA-RNA recombination of coronavirus in mouse brain. J. Virol. **62:**1810–1813.
16. **Keck, J. G., S. A. Stohlman, L. H. Soe, S. Makino, and M. M. C. Lai.** 1987. Multiple recombination sites at the 5′-end of murine coronavirus RNA. Virology **156:**331–341.
17. **Kumanishi, T.** 1967. Brain tumors induced with Rous sarcoma virus, Schmidt-Ruppin strain. I. Induction of brain tumors in adult mice with Rous chicken sarcoma cells. Jpn. J. Exp. Med. **37:**461–474.
18. **Lai, M. M. C.** 1990. Coronavirus: organization, replication and expression of genome. Annu. Rev. Microbiol. **44:**303–333.
19. **Lai, M. M. C., R. S. Baric, P. R. Brayton, and S. A. Stohlman.** 1984. Characterization of leader RNA sequences on the virion and mRNAs of mouse hepatitis virus, a cytoplasmic RNA virus. Proc. Natl. Acad. Sci. USA **81:**3626–3630.
20. **Lai, M. M. C., R. S. Baric, S. Makino, J. G. Keck, J. Egbert, J. L. Leibowitz, and S. A. Stohlman.** 1985. Recombination between nonsegmented RNA genomes of murine coronavi-

ruses. J. Virol. **56**:449–456.
21. **Lai, M. M. C., P. R. Brayton, R. C. Armen, C. D. Patton, C. Pugh, and S. A. Stohlman.** 1981. Mouse hepatitis virus A59: mRNA structure and genetic localization of the sequence divergence from hepatotropic strain MHV-3. J. Virol. **39**:823–834.
22. **Lai, M. M. C., C. D. Patton, R. S. Baric, and S. A. Stohlman.** 1983. Presence of leader sequences in the mRNA of mouse hepatitis virus. J. Virol. **46**:1027–1033.
23. **Lai, M. M. C., and S. A. Stohlman.** 1978. RNA of mouse hepatitis virus. J. Virol. **26**:236–242.
24. **Lee, H.-J., C.-K. Shieh, A. E. Gorbalenya, E. V. Eugene, N. La Monica, J. Tuler, A. Bagdzhadzhyan, and M. M. C. Lai.** 1991. The complete sequence (22 kilobases) of murine coronavirus gene 1 encoding the putative proteases and RNA polymerase. Virology **180**:567–582.
25. **Leibowitz, J. L., K. C. Wilhelmsen, and C. W. Bond.** 1981. The virus-specific intracellular RNA species of two murine coronaviruses: MHV-A59 and MHV-JHM. Virology **114**:39–51.
26. **Makino, S., J. O. Fleming, J. G. Keck, S. A. Stohlman, and M. M. C. Lai.** 1987. RNA recombination of coronaviruses: localization of neutralizing epitopes and neuropathogenic determinants on the carboxyl terminus of peplomers. Proc. Natl. Acad. Sci. USA **84**:6567–6571.
27. **Makino, S., N. Fujioka, and K. Fujiwara.** 1985. Structure of the intracellular defective viral RNAs of defective interfering particles of mouse hepatitis virus. J. Virol. **54**:329–336.
28. **Makino, S., M. Joo, and J. K. Makino.** 1991. A system for study of coronavirus mRNA synthesis: a regulated, expressed subgenomic defective interfering RNA results from intergenic site insertion. J. Virol. **65**:6031–6041.
29. **Makino, S., J. G. Keck, S. A. Stohlman, and M. M. C. Lai.** 1986. High-frequency RNA recombination of murine coronaviruses. J. Virol. **57**:729–737.
30. **Makino, S., and M. M. C. Lai.** 1989. High-frequency leader sequence switching during coronavirus defective interfering RNA replication. J. Virol. **63**:5285–5292.
31. **Makino, S., C.-K. Shieh, J. G. Keck, and M. M. C. Lai.** 1988. Defective-interfering particles of murine coronaviruses: mechanism of synthesis of defective viral RNAs. Virology **163**:104–111.
32. **Makino, S., C.-K. Shieh, L. H. Soe, S. C. Baker, and M. M. C. Lai.** 1988. Primary structure and translation of a defective interfering RNA of murine coronavirus. Virology **166**:550–560.
33. **Makino, S., F. Taguchi, and K. Fujiwara.** 1984. Defective interfering particles of mouse hepatitis virus. Virology **133**:9–17.
34. **Makino, S., F. Taguchi, N. Hirano, and K. Fujiwara.** 1984. Analysis of genomic and intracellular viral RNAs of small plaque mutants of mouse hepatitis virus, JHM strain. Virology **139**:138–151.
35. **Makino, S., K. Yokomori, and M. M. C. Lai.** 1990. Analysis of efficiently packaged defective interfering RNAs of murine coronavirus: localization of a possible RNA-packaging signal. J. Virol. **64**:6045–6053.
36. **Mann, R., and D. Baltimore.** 1985. Varying the position of a retrovirus packaging sequence results in the encapsidation of both unspliced and spliced RNAs. J. Virol. **54**:401–407.
37. **Mann, R., R. Mulligan, and D. Baltimore.** 1983. Construction of a retrovirus packaging mutant and its use to produce helper-free defective retrovirus. Cell **33**:153–159.
38. **Ollis, D. L., and S. W. White.** 1987. Structural basis of protein-nucleic acid interactions. Chem. Rev. **87**:981–995.
39. **Pugatsch, T., and D. W. Stacey.** 1983. Identification of a sequence likely to be required for avian retroviral packaging. Virology **128**:505–511.
40. **Sambrook, J., E. F. Fritsch, and T. Maniatis.** 1989. Molecular cloning: a laboratory manual, 2nd ed. Cold Spring Harbor Laboratory, Cold Spring Harbor, N.Y.
41. **Sawicki, S. G., and D. L. Sawicki.** 1986. Coronavirus minus-strand RNA synthesis and effect of cycloheximide on coronavirus RNA synthesis. J. Virol. **57**:328–334.
42. **Sethna, P. B., M. A. Hofmann, and D. A. Brian.** 1991. Minus-strand copies of replicating coronavirus mRNAs contain antileaders. J. Virol. **65**:320–325.
43. **Sorge, J., R. Ricci, and S. H. Hughes.** 1983. *cis*-acting RNA packaging locus in the 115-nucleotide direct repeat of Rous sarcoma virus. J. Virol. **48**:667–675.
44. **Spaan, W., H. Delius, M. Skinner, J. Armstrong, P. Rottier, S. Smeekens, B. A. M. van der Zeijst, and S. G. Siddell.** 1983. Coronavirus mRNA synthesis involves fusion of non-contiguous sequences. EMBO J. **2**:1939–1944.
45. **Stohlman, S. A., R. S. Baric, G. N. Nelson, L. H. Soe, L. M. Welter, and R. J. Deans.** 1988. Specific interactions between coronavirus leader RNA and nucleocapsid protein. J. Virol. **62**:4288–4295.
46. **Stohlman, S. A., and M. M. C. Lai.** 1979. Phosphoproteins of murine hepatitis virus. J. Virol. **32**:672–675.
47. **Sturman, L. S., K. V. Holmes, and J. Behnke.** 1980. Isolation of coronavirus envelope glycoproteins and interaction with the viral nucleocapsid. J. Virol. **33**:449–462.
48. **van der Most, R. G., P. J. Bredenbeek, and W. J. M. Spaan.** 1991. A domain at the 3′ end of the polymerase gene is essential for encapsidation of coronavirus defective interfering RNAs. J. Virol. **65**:3219–3226.
49. **Weber, K., and W. Konigsberg.** 1975. Proteins of the RNA phages, p. 51–84. *In* N. D. Zinder (ed.), RNA phages. Cold Spring Harbor Laboratory, Cold Spring Harbor, N.Y.
50. **Wei, N., L. A. Heaton, T. J. Morris, and S. C. Harrison.** 1990. Structure and assembly of turnip crinkle virus. VI. Identification of coat protein virus binding sites on the RNA. J. Mol. Biol. **214**:85–95.
51. **Weiss, B., H. Nitschko, I. Ghattas, R. Wright, and S. Schlesinger.** 1989. Evidence for specificity in the encapsidation of Sindbis virus RNAs. J. Virol. **63**:5310–5318.
52. **Zuker, M., and P. Steigler.** 1981. Optimal computer folding of large RNA sequences using thermodynamics and auxiliary information. Nucleic Acids Res. **9**:133–148.